STOCHASTIC 2-D MODELS OF GALAXY DISK EVOLUTION. THE GALAXY M33

T. Mineikis[1,2] and V. Vansevičius[1,2]

[1] *Vilnius University Observatory, Čiurlionio 29, Vilnius LT-03100, Lithuania; vladas.vansevicius@ff.vu.lt*

[2] *Center for Physical Sciences and Technology, Savanorių 231, Vilnius LT-02300, Lithuania; tadas.mineikis@ftmc.lt*

Abstract. We have developed a fast numerical 2-D model of galaxy disk evolution (resolved along the galaxy radius and azimuth) by adopting a scheme of parameterized stochastic self-propagating star formation. We explore the parameter space of the model and demonstrate its capability to reproduce 1-D radial profiles of the galaxy M33: gas surface density, surface brightness in the i and GALEX *FUV* passbands, and metallicity.

Key words: galaxies: evolution – galaxies: individual (M 33)

1. INTRODUCTION

Numerous recent resolved photometric and spectroscopic surveys of galaxies allow us to explore a two-dimensional (2-D) structure of galaxy disks (resolved along the galaxy radius and azimuth) in detail. Studies of disk structures have proved them to be feature-rich (e.g., Bastian et al. 2007; Gieles et al. 2008; Bastian et al. 2009; Sanchez et al. 2010). On the other hand, simulations of galaxy disks with hydrodynamical models are computationally costly and dependent on the parametrization of sub-grid physics and even on the implementation methods (Scannapieco et al. 2012). Additionally, in the cases of late-type spirals fine tuning of the models is needed (Roškar et al. 2014, and references therein). An increased spatial resolution of the simulations could be the key to the problem, however, this would make galaxy models computationally even more daunting (Guedes et al. 2011).

In the past, there was an attempt to create fast semi-analytic 2-D models of galactic disks, based on a stochastic self-propagating star formation (SPSF) scenario (Seiden & Gerola 1982, and references therein). The SPSF approach was shown to be suitable to form flocculent spiral arms reminiscent of late-type spirals (Gerola & Seiden 1978). The properties of dwarf galaxies (Gerola et al. 1980), as well as larger spirals (Feitzinger et al. 1981), were explained by employing the SPSF scenario. Despite further developments of the grid-free SPSF variants (Jungiewert & Palouš 1994; Sleath & Alexander 1995), galaxy modeling shifted towards N-body and hydrodynamical approaches.

In this study we present an updated version of the 2-D stochastic galaxy disk

model by Mineikis & Vansevičius (2010). The most important new features of the updated version are the implementation of the radial profile of gas accretion onto the disk, based on the present-day mass distribution in the galaxy M33, and the stellar "dispersion" across the disk. These features allow us to produce realistic radial profiles of the surface brightness. We also improved the model by minimizing a number of free parameters and designing it for fast generation of the results of resolved stellar photometry.

In order to verify the model, we explored an extensive grid of parameters by comparing the model generated radial profiles of one-dimensional (1-D) galaxy disk with the observed ones. For the study we used the well explored Local Group galaxy M33. The relatively unperturbed stellar disk (Ferguson et al. 2007) and its favorable inclination together with the small distance – 840 kpc (Freedman et al. 2001), as well as the low Galactic extinction in its direction, makes this galaxy one of the best laboratories for studies of the SPSF scenario. M33 has the characteristic flocculent spiral arms inherent to the late-type disk galaxies. Although two spiral arms are visible in the near infrared (Regan & Vogel 1994), they do not dominate the present-day star formation pattern, as can be seen on the far ultraviolet and Hα images (Thilker et al. 2005). The abundance of observational data makes the M33 galaxy the best target to test our 2-D model.

The article is organized as follows. In Section 2 we describe the model, in Section 3 the model parameters are calibrated for the galaxy M33, a discussion of the simulation results is given in Section 4 and, finally, in Section 5 the conclusions are presented.

2. THE MODEL

2.1. Disk geometry and time step

The disk model is divided into $N_{\rm R}$ rings of equal width (Mineikis & Vansevičius 2010). Each ring is subdivided into cells, which are the smallest elements of the model. This subdivision follows the rule that the ring with the running number i has $6 \cdot i$ cells, producing a total of $3N_{\rm R}(N_{\rm R} - 1) + 1$ cells in the disk. This subdivision results in equal area cells, except for the central one, which is smaller by a factor of $3/4$. The physical size of the disk model is defined by the physical size of cells and the number of rings.

We assume the size of cells to be comparable to the typical size of OB associations. According to the recent findings by Bastian et al. (2007), star formation (SF) is a hierarchical scale-free process, highly dependent on the definitions. Nevertheless, our model is not very sensitive to the adopted cell size, therefore, in this study, a cell size is set to $d_{\rm C} = 100$ pc.

The model integration time step ($\Delta t_{\rm I}$) corresponds to the SF propagation time across the cell. We assume that the SF propagation velocity is $v_{\rm SF} = 10$ km/s (Feitzinger et al. 1981), i.e., it corresponds to the typical speed of sound in the interstellar matter within a cell, therefore:

$$\Delta t_{\rm I} = 10 \text{ Myr} \cdot \frac{d_{\rm C}}{100 \text{ pc}} \cdot \left(\frac{v_{\rm SF}}{10 \text{ km/s}} \right)^{-1}. \tag{1}$$

2.2. Gas accretion

Although mass accretion histories of dark matter (DM) halos are highly variable (McBride et al. 2009), they tend, on average, to obey simple relations. McBride et al. (2009) studied the Millennium simulation data and found a simple empirical fit to the average DM accretion rate. The fit relates the mean accretion rate of DM to a given halo mass at a given redshift. Using the higher resolution Millennium II simulation, Fakhouri et al. (2010) confirmed the validity of the fit and extended it to smaller halo masses. We use the results by Fakhouri et al. (2010) to prescribe the DM and, correspondingly, baryonic mass (BM) build-up of the model.

The gas falling into the DM halo is distributed in the thin disk. The radial profile of the accretion is assumed to be a scaled version of the total BM radial profile of the present-day galaxy disk:

$$A_{\mathrm{G}}(r,t) = \frac{B(r)}{2\pi \int_0^R B(r)r\mathrm{d}r} \cdot A_{\mathrm{DM}}(t) \cdot \beta, \qquad (2)$$

where $A_{\mathrm{G}}(r,t)$ is the radial profile of gas accretion rate, $B(r)$ is the radial profile of BM density in the galaxy disk, $A_{\mathrm{DM}}(t)$ is the rate of DM accretion on the galaxy halo, and $\beta = \Omega_{\mathrm{BM}}/\Omega_{\mathrm{DM}}$ is the primordial ratio of BM to DM. Such a definition of accretion guarantees the build-up of the present-day disk over the galaxy's life-time. The metallicity of the accreted gas is set to $Z_{\mathrm{A}} = 0.0001$.

2.3. Star formation

The star formation process in the disk is modeled by discrete SF events occurring stochastically in the cells. The cell can experience a SF event spontaneously (probability P_{S}) or be triggered (probability P_{T}).

• *Spontaneous SF probability P_{S}*: this parameter defines SF events occurring stochastically in the cells without any external influence. The spontaneous SF sustains SF activity in the disk. In this study we set P_{S} to be very small, i.e., ∼1 SF event per model integration time-step Δt_{I} over the whole disk. Additionally, we assume that spontaneous SF events are more probable in the cells possessing higher gas density: $P_{\mathrm{S}} \propto \Sigma_{\mathrm{G}}^2$, where Σ_{G} is a surface gas density within a cell.

• *Triggered SF probability P_{T}*: this parameter represents a chain of complex processes in the cell's interstellar medium (molecular cloud) after the SF event has occurred. A molecular cloud will undergo imminent disruption by an energetic feedback of stellar winds, expanding H II zones and supernovae explosions. Despite a negative SF feedback locally (on a scale of cell), SF could be triggered on a larger scale (i.e., in neighboring cells). For the cell i, which experiences a SF event in a time step t_k, the neighboring cell j, being in direct contact with the cell i, can experience a SF event during the next time step t_{k+1} with a probability of $P_{\mathrm{T},j}$.

At the start of galaxy simulation the SF in the disk is inhibited by the critical gas surface density Σ_{C}. If the gas surface density in a cell is below critical, the probability of SF event is reduced by a factor of $\Sigma_{\mathrm{G}}/\Sigma_{\mathrm{C}}$. As the simulation evolves, the gas density in the disk increases and SF becomes more probable starting from the inner disk parts. In the outer disk, Σ_{G} remains small, compared to Σ_{C}, for a longer time and defines the extent of the SF disk. We note that Σ_{C} defines the local density, i.e., not averaged azimuthally, as this parameter is usually derived from observations.

Table 1. PEGASE-HR parameters used to generate SSPs.

Parameter	Value	Reference
Stellar library	low-resolution	Le Borgne et al. (2004)
Initial mass function	corrected for binnaries	Kroupa (2002)
Fraction of close binaries	0.05	default PEGASE-HR value
Ejecta of massive stars	type B	Woosley & Weaver (1995)
Nebular emission	true	PEGASE-HR value

During a SF event, a fraction of gas available in a cell is converted to stars. This fraction is called the SF efficiency, SFE:

$$\text{SFE} = \epsilon \cdot \left(\frac{\Sigma_{\text{G}}}{10 \ M_{\odot}/\text{pc}^2} \right)^{\alpha}, \tag{3}$$

where ϵ and α are free parameters. In order to avoid generating unrealistic stellar populations of extremely low mass or SFE exceeding 100%, we set the lower and upper SFE cut-offs to 0.05% and 50%, respectively. Additionally, if the stellar population, born in a cell, is less massive than $100 \, M_{\odot}$, we assume that the starburst does not trigger neighboring cells because the population is, on average, lacking supernovae.

2.4. The evolution of cells

Each stellar population, formed in a cell during a SF event, could be well represented by a simple stellar population (SSP). To track the entire SF history of a cell, the value of mass of each particular stellar population is stored in a 2-D (age vs. metallicity) array, S. The step in age, t_{S}, can be set in accordance to the size of a cell (10 Myr throughout the paper). The step in metallicity (0.1–0.3 dex) is predefined by the used dataset of interpolated isochrones. To track the evolution of SSPs self-consistently, we employ the package PEGASE-HR (Le Borgne et al. 2004; see Table 1 for the parameters used).

The stars from any SSP, formed in a cell, can move to the neighboring cell, therefore, arrays S_j of the neighboring cells have to be modified accordingly. Stellar spread to neighboring cells is implemented as a "dispersion" process. The evolution of the stellar content in the cell S_i is given by

$$\frac{\Delta S_i}{\Delta t} = \Psi_i - D_{\text{S}} \cdot \sum_j \lambda_{i,j} \cdot (S_i - S_j), \tag{4}$$

where Ψ_i is the mass of a newly formed SSP, D_{S} is the "dispersion" constant, $\lambda_{i,j}$ is the length of borderline between cell i and its neighbors j. To prevent star flow anisotropies near the center of galaxy, which occur due to change in the length ratios of the cell sides, we correct corresponding λ to keep star flows through each side of the cell equal.

The evolution of gas content in the cell G_i is given taking into account SSP evolution:

$$\frac{\Delta G_i}{\Delta t} = -\Psi_i + A_i - \sum_j F_{i,j} + \sum_k \sum_l (S_i \circ R)_{k,l}, \tag{5}$$

where A_i is the accreted gas mass, $F_{i,j}$ are the gas mass flows (see Section 2.5) between cell i and neighboring cells j, and R is the array representing the mass

fraction of stellar populations returned to gaseous content, i.e., the last term[1] represents the total gas mass returned to gas pool of the cell i by stellar populations evolving within this cell (the indices k and l denote the age and metallicity).

The metallicity (Z_i) evolution of the gas content in the i-th cell is given by

$$\frac{\Delta(Z_i \cdot G_i)}{\Delta t} = -\Psi_i \cdot Z_i + A_i \cdot Z_A - \sum_j F_{i,j} \cdot Z_j + \sum_k \sum_l (S_i \circ Z)_{k,l}, \qquad (6)$$

where Z_A represents the metallicity of the accreting gas, j denotes the neighboring cells, and Z is the array representing yields of metals returned to the gas pool of the i-th cell by stellar populations evolving within this cell.

2.5. Gas flows

Due to the small size ($\sim 100 \times 100$ pc) of cells covering the galaxy disk, gas masses are expected to flow beyond the cells in one time step. The main structures causing gas movement are superbubbles inflated by SF feedback. Following the formulation by Castor et al. (1975), on time-scale of 10 Myr superbubbles reach ~ 100 pc in size for a typical gas density of $20\,M_\odot/\mathrm{pc}^2$ and SFE values of a few percent. Therefore, a cell experiencing a SF event on a time-scale of 10 Myr will be filled with hot tenuous gas, causing a large part of the gas to move out of the cell.

After 40 Myr, when supernovae vanish and the superbubble inflated cavity cools down, the gas returns to the cell. The force driving the gas to refill the cell is the random motion of H I gas clouds having typical velocities of ~ 10 km/s (see, e.g., Corbelli & Schneider (1997) for the galaxy M33). Based on the arguments by Hunter & Gallagher (1990), we estimate the refill time-scale $\tau = d_C/(2\cdot 10 \text{ km/s}) \simeq 50$ Myr.

We implemented both types of gas flows in the galaxy disk model: expulsion by a SF event and refilling.

• *Gas expulsion*: this is implemented simply by moving gas from the cell i, experiencing a SF event, to the neighboring cells j. The gas flows only to those neighbors which have had no a SF event for the past 40 Myr:

$$F_{i,j} = \lambda_{i,j} \cdot \begin{cases} 0 & \Delta_{\mathrm{SF},j} \leq 40\,\mathrm{Myr} \\ G_i & \Delta_{\mathrm{SF},j} > 40\,\mathrm{Myr}, \end{cases} \qquad (7)$$

where gas flows between cells $F_{i,j}$ depend on the length, $\lambda_{i,j}$, of the borderline, and G_i is the gas mass remaining in the cell i after the SF event. The flow occurs within one time step after the SF event.

• *Gas refilling*: this is implemented under the assumption that equilibrium gas distribution in the galaxy follows the present-day baryonic matter distribution $B(r)$, i.e., any deviation from it, ($G(r_i)/G(r_j) \neq B(r_i)/B(r_j)$), generates gas flows between cells on the time-scale τ:

$$F_{i,j} = \lambda_{i,j} \cdot \frac{1}{\tau} \cdot \frac{G(r_j) \cdot B(r_i) - G(r_i) \cdot B(r_j)}{B(r_i) + B(r_j)}. \qquad (8)$$

---

[1] Also known as Hadamard (or Schur) product, for two matrices of the same dimension, $(B \circ C)_{k,l} = B_{k,l} \cdot C_{k,l}$

Table 2. The parameters of the 2-D galaxy model.

Parameter	Notation	Value
Fixed parameters		
Age	–	13 Gyr
Baryonic mass	–	$1.1 \cdot 10^{10} \, M_\odot$
Disk radius	–	12 kpc
Disk rotation	–	Corbelli & Salucci (2007)
Cell size	d_C	100 pc
SF propagation speed	v_SF	10 km/s
Accretion rate	$A_\mathrm{DM}(t)$	Fakhouri et al. (2010)
Critical gas surface density	Σ_C	$8 \, M_\odot/\mathrm{pc}^2$
Gas refilling time-scale	τ	50 Myr
Star "dispersion" constant	D_S	$200 \, \mathrm{pc}^2/\mathrm{Myr}$
Spontaneous SF probability	P_S	1 SF region per Δt_I
Varied parameters		
Triggered SF probability	P_T	0.28-0.44
SF efficiency	ϵ	$(0.018\text{-}5.7)\cdot10^{-2}$
SF power index	α	1.5-2.5

3. THE MODEL SETUP FOR M33

The model parameters used for the M33 galaxy simulation are given in Table 2. The model disk (radius of 12 kpc) comfortably engulfs the star forming disk of M33. The presence of the RR Lyr variables in M33 (Pritzl et al. 2011 and references therein) implies its old age, therefore, the galaxy formation was assumed to start 13 Gyr ago. The critical gas density for SF (Σ_C) was suggested to be in the range 3–$10 \, M_\odot/\mathrm{pc}^2$ (Schaye 2004). We have found that lower end values do not change the simulation results significantly and adopted $\Sigma_\mathrm{C} = 8 \, M_\odot/\mathrm{pc}^2$. The 1-D radial profiles are not very sensitive to the stellar "dispersion" parameter, therefore, it was set to $200 \, \mathrm{pc}^2/\mathrm{Myr}$. The effects of this "dispersion" parameter will be analyzed in the subsequent paper devoted to the study of properties of 2-D galaxy models.

An assumption was made that the radial profile of gas accretion is a scaled version of the radial profile of total baryonic mass (gaseous and stellar) in the galaxy. To avoid computationally expensive iterative fitting of baryonic mass for each model, we derived the radial profile by performing the decomposition of the galaxy's rotation curve. The observational data of the rotation curve were taken from Corbelli & Salucci (2007). The rotation curve was decomposed into four mass components: gaseous disk, stellar nucleus, exponential stellar disk and pseudo-isothermal DM halo.

The contribution of the gas disk to the rotation curve was calculated by co-adding H I and H$_2$ data from Corbelli & Salucci (2000) and Heyer et al. (2004), respectively. Helium mass fraction was taken into account by multiplying hydrogen gas mass by a factor of 1.33. Corbelli (2003) has established that the mass of the M33 stellar nucleus is in the interval $(0.3-8)\cdot10^8 \, M_\odot$, therefore, in order to narrow a free-parameter space, we assume that the stellar nucleus is a point source with a mass of $10^8 \, M_\odot$. To avoid the effects of the extended nucleus, we did not fit the innermost 0.5 kpc part of the rotation curve.
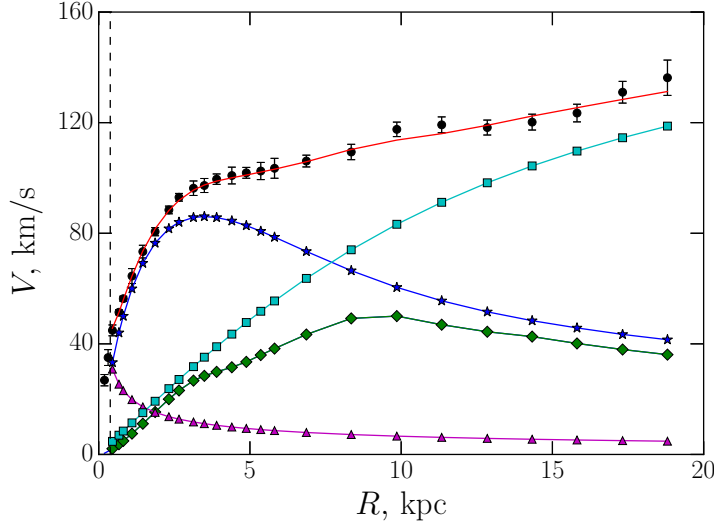
Fig. 1. Circular speed versus radius for the galaxy M33. The black dots with error bars indicate the observed rotation curve (Corbelli & Salucci 2007). The red line is the best-fitting model rotation curve (see the text for the model description). Individual contributions from the components are also shown: pseudo-isothermal DM halo (cyan squares), exponential stellar disk (blue stars), gaseous disk (green diamonds) and stellar nucleus (magenta triangles).

We fitted the following two components:

- a pseudo-isothermal DM halo with the core radius R_c and the asymptotic rotation velocity $V_R(\infty)$, e.g., de Blok et al. (2008);

- an exponential stellar disk with the central surface density Σ_S and the scale length R_e. The stellar disk was assumed to have a scale height of 100 pc.

Dynamical contributions of gaseous and stellar disk components were computed using the task *rotmod* within the software package GIPSY (van der Hulst et al. 1992) which implements the method of Cesartano (1983). For each pair of the parameters describing the stellar disk, Σ_S & R_e, we minimized χ^2 by fitting the DM radial profile.

The best fitted rotation curve with $R_e = 1.57$ kpc, $\Sigma_S = 470\, M_\odot/\mathrm{pc}^2$, $R_c = 10.2$ kpc, and $V_R(\infty) = 184$ km/s is shown in Fig. 1. The derived scale length of stellar disk is in agreement with the values derived photometrically, 1.4 kpc in the K-passband for the inner 4 kpc of M33 (Regan & Vogel 1994) and 1.5–1.6 kpc in the Spitzer passbands at 3.4 and 4.5 μm (Verley et al. 2009). The best-fitted stellar and gaseous disks were used to define the radial gas accretion profile of M33.

The grid of models was computed by varying the main SF parameters: ϵ, α and P_T. The grid is composed of 17 linear steps in P_T, 5 linear steps in α and 11 logarithmic steps in ϵ. In order to reduce stochastic effects, every model is presented as an average of six snapshots spaced by 200 Myr during the last 1 Gyr.
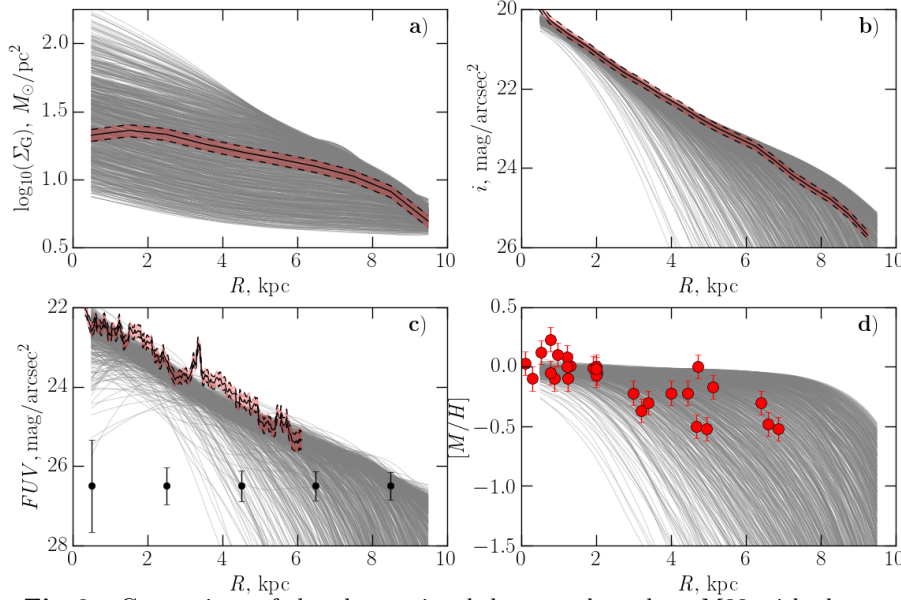
Fig. 2. Comparison of the observational data on the galaxy M33 with the models. The gas surface density (panel a) is computed by co-adding the radial profiles of H I (Corbelli & Salucci 2000) and H_2 (Heyer et al. 2004) gas surface density. The surface brightness radial profile in the i passband (panel b) (Ferguson et. al. 2007) is corrected for internal extinction using the radial extinction profile by Munoz-Mateos et al. (2007) and assuming the LMC-like extinction law (Gordon et al. 2003). The surface brightness radial profile in GALEX *FUV* passband (panel c) (Munoz-Mateos et al. 2007) is also corrected for internal extinction. The metallicity measurements of blue supergiant stars (panel d) are taken from Urbaneja et al. (2005) and U et al. (2009). All radial profiles of observed surface brightness are de-projected adopting 54° for the galaxy disk inclination.

4. RESULTS

Comparisons of the models with observational data for the galaxy M33 are presented in Fig. 2. The models are compared with 1-D radial profiles of: gas surface density (H I from Corbelli & Salucci 2000, H_2 from Heyer et al. 2004), surface brightness in i (Ferguson et al. 2007) and GALEX *FUV* (Munoz-Mateos et al. 2007) passbands, and metallicity (Urbaneja et al. 2005; U et al. 2009).

The gas surface density radial profile derived from observations constrains strongly the model parameter space due to large variation of the model gas density radial profiles, especially in the inner parts of the galaxy (Fig. 2, panel a).

The surface brightness radial profile in the i passband constrains well the stellar mass of the models. However, we set the same total mass for all models, thus there are no significant variations in the i passband radial profiles, except in the outer parts of the galaxy, where model radial profiles span a wide range (Fig. 2, panel b).

The GALEX *FUV* passband surface-brightness radial profile constrains well the SF rate along the model galaxy radius (Fig. 2, panel c). However, this profile is not very sensitive to the model parameters since the accretion time-scale exceeds the gas consumption time-scale, i.e., SF is gas-accretion regulated (Elmegreen 2014 and references therein).
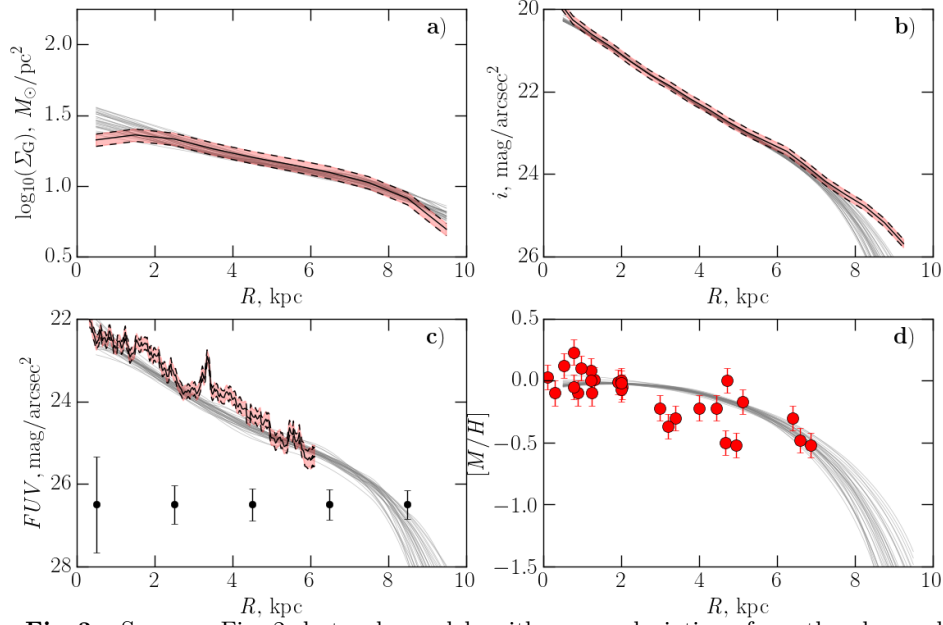
Fig. 3. Same as Fig. 2, but only models with r.m.s. deviations from the observed radial profiles (gas surface density and i passband) smaller than 10% and in the radial distance range 2–7 kpc are shown.
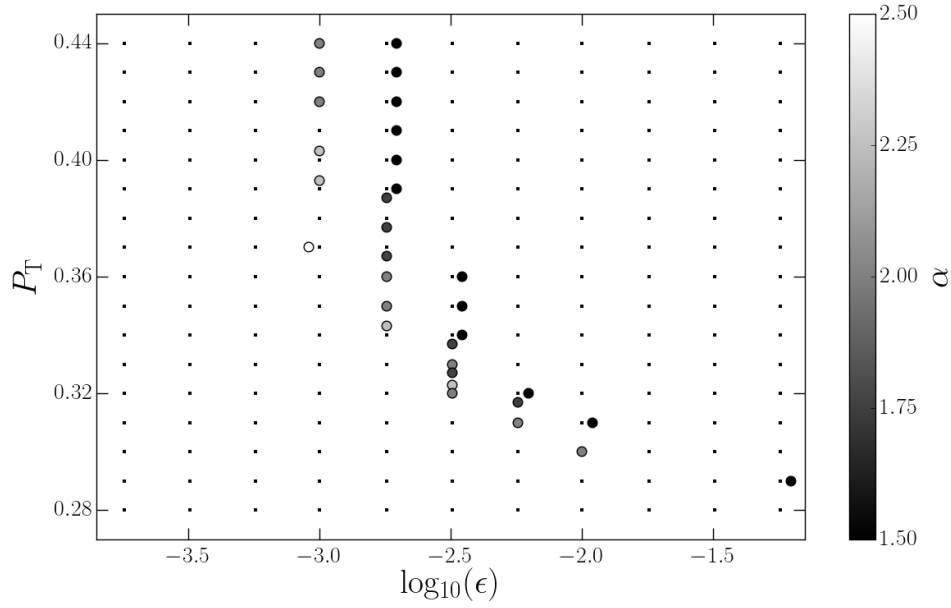

Fig. 4. 3-D parameter space of the models shown in Fig. 3. The gray-shaded circles indicate the values of α parameter. The small black points at each node of the model grid indicate a fully explored extent of the parameter space.
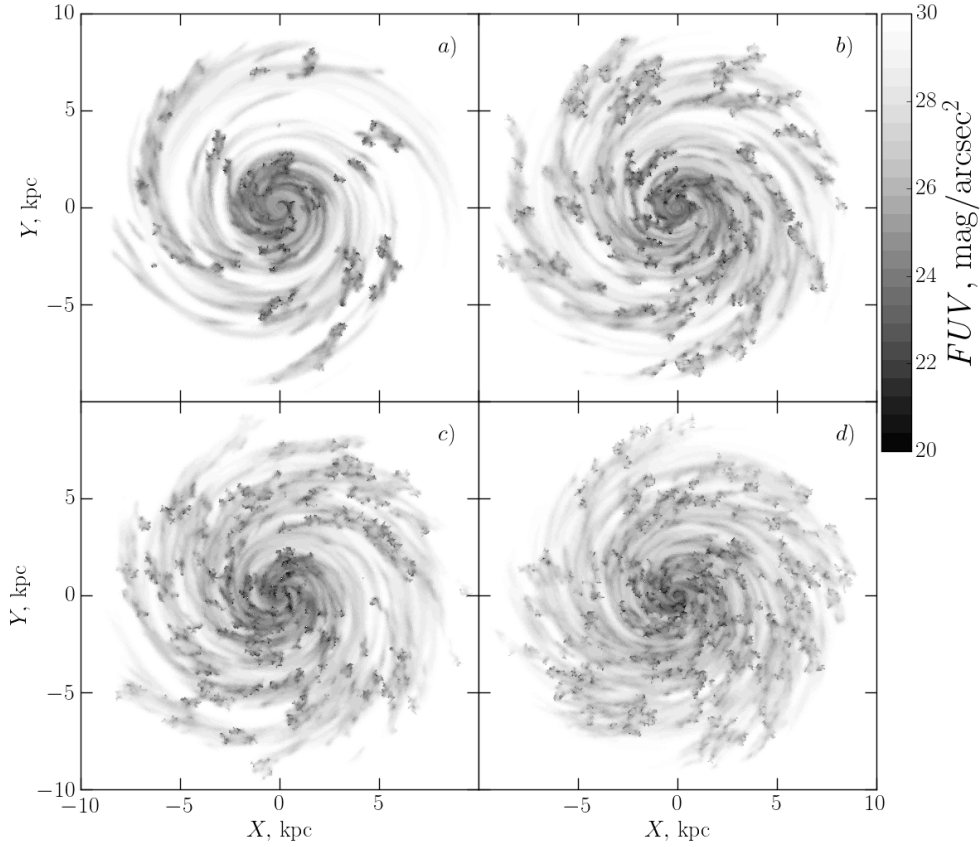
Fig. 5. The galaxy models from the "degeneracy valley" (Fig. 4) in the GALEX *FUV* passband: (a) $P_T = 0.30$, $\epsilon = 1\%$; (b) $P_T = 0.31$, $\epsilon = 0.6\%$; (c) $P_T = 0.32$, $\epsilon = 0.3\%$; (d) $P_T = 0.34$, $\epsilon = 0.2\%$. For all models, $\alpha = 2$. The models possess very similar 1-D radial profiles, but they demonstrate different 2-D patterns of the young SF regions.

The metallicity radial profiles (Fig. 2, panel d) are sensitive to the model parameters, however, they are of limited use because of large scatter in the observational data.

Therefore, to further constrain the model parameter space we used only the gas surface density and the i passband radial profiles. For each model we calculated the r.m.s. deviations from both observed radial profiles in the most reliable (for models) radial distance range, i.e., 2–7 kpc. The inner region of the model galaxy has an increasingly anisotropic grid and the outer parts are affected by the uncertainty in the critical gas surface density, Σ_C. In Fig. 3 we show the models selected by r.m.s. deviations from the observed radial profiles (gas surface density and i passband) being less than 10%.

The parameter space of the selected models is shown in Fig. 4. A prominent feature of this figure is the "degeneracy valley" – the region in the parameter space where reside the models selected by the 1-D radial profile procedure described above. The "degeneracy valley" is seen because the 1-D radial profiles are derived

by convolving the 2-D distributions of SF regions, e.g., SF in the model galaxy being smooth and inefficient or patchy and efficient would produce similar 1-D radial profiles.

This effect is shown in Fig. 5, where four different models taken from the "degeneracy valley" of Fig. 4 are plotted. Fig. 5 illustrates that, by increasing P_T and decreasing ϵ values, SF becomes more smooth. It is challenging to break those degeneracies by using only 1-D observed radial profiles, however, feature-rich 2-D model structures (Fig. 5) imply the possibility to solve this problem by employing spatially resolved observations of real galaxy disks.

5. CONCLUSIONS

We presented a 2-D model of galaxy disk evolution, based on the stochastic self-propagating star formation process. The parameterized gas and star dynamics, together with self-consistent chemical and photometric evolution of stellar populations, are implemented in the model. The galaxy build-up prescription is taken from the N-body DM simulations by Fakhouri et al. (2010).

We applied the model for the interpretation of observational data on the M33 galaxy and successfully reproduced the 1-D radial profiles of the gas surface density, GALEX *FUV* and *i* passband surface brightness, and stellar metallicity. We explored possible degeneracies of the model parameters by computing the extensive grid of models. We have found that observational data, averaged as 1-D radial profiles, cannot fully characterize galaxy evolution. In order to break the degeneracies, the analysis of 2-D SF region patterns is additionally required.

REFERENCES

Bastian N., Ercolano B., Gieles M. et al. 2007, MNRAS, 379, 1302
Bastian N., Gieles M., Ercolano B., Gutermuth R. 2009, MNRAS, 392, 868
Castor J., McCray R., Weaver R. 1975, ApJ, 200, L107
Casertano S. 1983, MNRAS, 203, 735
Corbelli E., Schneider S. E. 1997, ApJ, 479, 244
Corbelli E., Salucci P. 2000, MNRAS, 311, 441
Corbelli E. 2003, MNRAS, 342, 199
Corbelli E., Salucci P. 2007, MNRAS, 374, 1051
de Blok W. J. G., Walter F., Brinks E. et al. 2008, AJ, 136, 2648
Elmegreen B. G. 2014, arXiv:1410.1075
Fakhouri O., Ma C.-P., Boylan-Kolchin M. 2010, MNRAS, 406, 2267
Feitzinger J. V., Glassgold A. E., Gerola H., Seiden P. E. 1981, A&A, 98, 371
Ferguson A., Irwin M., Chapman S. et al. 2007, *Island Universes – Structure and Evolution of Disk Galaxies*, Springer, p. 239
Freedman W. L., Madore B. F., Gibson B. K. et al. 2001, ApJ, 553, 47
Gerola H., Seiden P. E. 1978, ApJ, 223, 129
Gerola H., Seiden P. E., Schulman L. S. 1980, ApJ, 242, 517
Gieles M., Bastian N., Ercolano B. 2008, MNRAS, 391, L93
Gordon K. D., Clayton G. C., Misselt K. A., Landolt A. U., Wolff, M. J. 2003,

ApJ, 594, 279

Guedes J., Callegari S., Madau P., Mayer L. 2011, ApJ, 742, 76

Heyer M. H., Corbelli E., Schneider S. E., Young J. S. 2004, ApJ, 602, 723

Hunter D. A., Gallagher J. S. III 1990, ApJ, 362, 480

Jungwiert B., Palous J. 1994, A&A, 287, 55

Kroupa P. 2002, Science, 295, 82

Le Borgne D., Rocca-Volmerange B., Prugniel P. et al. 2004, A&A, 425, 881

McBride J., Fakhouri O., Ma C.-P. 2009, MNRAS, 398, 1858

Mineikis T., Vansevičius V. 2010, Baltic Astronomy, 19, 111

Muñoz-Mateos J. C., Gil de Paz A., Boissier S. et al. 2007, ApJ, 658, 1006

Pritzl B. J., Olszewski E. W., Saha, A., Venn K. A., Skillman E. D. 2011, AJ, 142, 198

Regan M. W., Vogel S. N. 1994, ApJ, 434, 536

Roškar R., Teyssier R., Agertz O., Wetzstein M., Moore B. 2014, MNRAS, 444, 2837

Sánchez N., Añez N., Alfaro E. J., Crone Odekon M. 2010, ApJ, 720, 541

Scannapieco C., Wadepuhl M., Parry O. H. et al. 2012, MNRAS, 423, 1726

Schaye J. 2004, ApJ, 609, 667

Seiden P. E., Gerola H. 1982, Fundamentals of Cosmic Physics, 7, 241

Sleath J. P., Alexander P. 1995, MNRAS, 275, 507

Thilker D. A., Hoopes C. G., Bianchi L. et al. 2005, ApJL, 619, L67

Urbaneja M. A., Herrero A., Kudritzki R.-P. et al. 2005, ApJ, 635, 311

U V., Urbaneja M. A., Kudritzki R.-P. et al. 2009, ApJ, 704, 1120

van der Hulst J. M., Terlouw J. P., Begeman K. G., Zwitser W., Roelfsema P. R. 1992, Astronomical Data Analysis Software and Systems I, 25, 131

Verley S., Corbelli E., Giovanardi C., Hunt L. K. 2009, A&A, 493, 453

Woosley S. E., Weaver T. A. 1995, ApJS, 101, 181